Title	Dual-band antenna with compact radiator for 2.4/5.2/5.8 GHz WLAN applications
Author(s)	Sun, X; Cheung, SW; Yuk, TTI
Citation	IEEE Transactions on Antennas and Propagation, 2012, v. 60 n. 12, p. 5924-5931
Issued Date	2012
URL	http://hdl.handle.net/10722/189077
Rights	IEEE Transactions on Antennas and Propagation. Copyright © IEEE.

Dual-Band Antenna With Compact Radiator for 2.4/5.2/5.8 GHz WLAN Applications

Xiao Lei Sun, Li Liu, S. W. Cheung, *Senior Member, IEEE*, and T. I. Yuk, *Member, IEEE*

***Abstract*—This paper presents a dual-band planar antenna with a compact radiator for 2.4/5.2/5.8-GHz wireless local area network (WLAN) applications. The antenna consists of an L-shaped and E-shaped radiating elements to generate two resonant modes for dual-band operation. The L-element fed directly by a 50-Ω microstrip line is designed to generate a frequency band at around 5.5 GHz to cover the two higher bands of the WLAN system (using the IEEE 802.11a standard). The E-element is coupled-fed through the L-element and designed to generate a frequency band at 2.44 GHz to cover the lower band of the WLAN system (using the 802.11 b/g standards). As a result, the L- and E-elements together are very compact with a total area of only $8 \times 11.3\ \mathrm{mm}^2$. Parametric study on the key dimensions is investigated using computer simulation. For verification of simulation results, the antenna is fabricated on a $40 \times 30 \times 0.8\ \mathrm{mm}^3$ substrate and measured. The effects of the feeding cable used in the measurement system and the housing and liquid crystal display of wireless devices on the return loss, radiation pattern, gain and efficiency are also investigated by computer simulation and measurement.**

***Index Terms*—Cable effects, coupled-fed, dual band, E-shaped radiating element, L-shaped radiating element, wireless local area network (WLAN).**

I. Introduction

CURRENTLY, the wireless local area network (WLAN) is one of the most popular networks for accessing the internet. The WLAN uses a lower frequency band, 2.4–2.484 GHz, for the 802.11b/g standards, and two higher frequency bands, 5.15–5.35 GHz and 5.725–5.825 GHz, for the 802.11a standard. As the demand for smaller sizes of wireless devices increases, antennas designers are making tremendous efforts in attempts to reduce the physical sizes of the antennas, yet covering all the three operation bands. A simple method used in WLAN antennas to cover the three bands is to use one monopole for the lower band and another monopole or a branch structure for the two higher bands [1]–[9]. However, due to the required length of monopole for resonating in the lower band, this method leads to a relatively large antenna size. Different techniques have been proposed to reduce the size of the monopole responsible for the lower band. For example, in [1]–[7], the monopoles responsible for the lower band were bent to different shapes for size reduction. The smallest size achieved was with the use of a FR4 substrate (with a relative permittivity $\varepsilon_r = 4.4$) and $15 \times 10\ \mathrm{mm}^2$ [3], which is still larger than our proposed antenna of only $8 \times 11.3\ \mathrm{mm}^2$.

There are also other designs of antennas for WLAN applications. For example, in [10], a split-ring was used as a monopole radiator to generate dual-band operation. The design achieved a size of $16 \times 13\ \mathrm{mm}^2$ when fabricated on a substrate with a large $\varepsilon_r = 6.15$. An interesting design for WLAN application was reported in [11], where dual-band operation was achieved by combining two loop antennas together. However, the element was quite large because both loops required operating in the one-wavelength resonant modes. In [12], a slot was cut on the ground plane to generate the higher band for the WLAN system and the ground plane itself resonated in the lower band. Thus, the antenna size, including the large ground plane, was quite large about $34 \times 11.5\ \mathrm{mm}^2$. In [13], a pair of symmetrical horizontal strips embedded in a slot on the ground plane was used to excite a dual-band resonance. The slot occupied a large area of about $30 \times 14\ \mathrm{mm}^2$.

The size of the antenna for the WLAN system is mainly determined by the lower band at 2.4 GHz and there are techniques to reduce the size of the radiating element. Among many techniques, inverted-F structure is an effective one [14]–[17]. However, for multiband operation, the antenna needs to have more radiating elements, other than the inverted-F element. Thus the design challenge is to incorporate the inverted-F element with other radiating elements, yet maintaining the compact size. To tackle this challenge, in [18], the antenna employed a direct-fed inverted-F element for the 2.4-GHz band and two other long slots on the ground plane to generate the 5.2/5.8-GHz and 3.5-GHz bands. The inverted-F element had a very compact area of $6 \times 13\ \mathrm{mm}^2$, but the overall size of the antenna was much larger due to the slots on the ground plane. In [19], a direct-fed planar inverted-F antenna (PIFA) combined with a parasitic element was proposed for WLAN applications. The PIFA resonated in the fundamental mode at 2.4 GHz and the second-order mode at 5.2 GHz. The parasitic element with one end shorted to ground was used to generate the 5.8-GHz band. The radiator of the antenna had a compact size of $16.5(\mathrm{L}) \times 11.5(\mathrm{W}) \times 5(\mathrm{H})\ \mathrm{mm}^3$. Although the height had been reduced compared with other PIFA antennas, the antenna was rather high profile and still occupied a larger volume than a planar antenna due to the PIFA structure.

In this paper, a planar dual-band antenna using a very compact radiator ($8 \times 11.3\ \mathrm{mm}^2$) to cover all the 2.4/5.2/5.8 GHz WLAN operating bands is proposed. The radiator consists of an L-shaped and E-shaped elements resonating at around 5.5 and 2.44 GHz, respectively. The L-element is microstrip fed. However, the E-element is placed very close to the L-element

Manuscript received December 22, 2011; revised June 14, 2012; accepted July 10, 2012. Date of publication August 02, 2012; date of current version November 29, 2012.

The authors are with the Department of Electrical and Electronic Engineering, The University of Hong Kong, Hong Kong (e-mail: xlsun@eee.hku.hk; liuli@eee.hku.hk; swcheung@eee.hku.hk; tiyuk@eee.hku.hk).

Color versions of one or more of the figures in this paper are available online at http://ieeexplore.ieee.org.

Digital Object Identifier 10.1109/TAP.2012.2211322

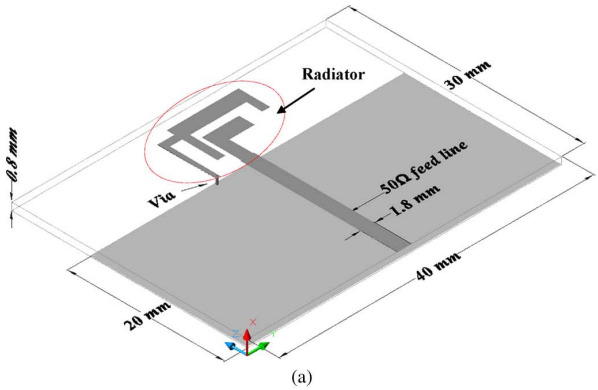

(a)

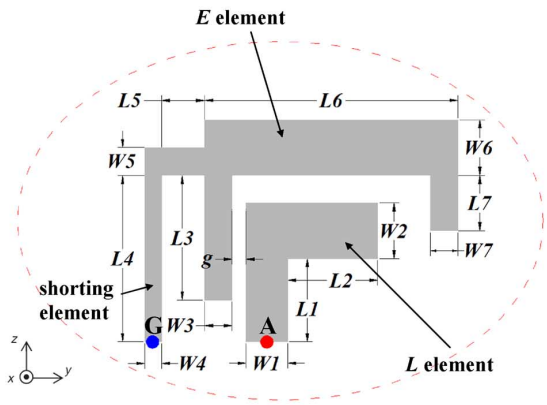

(b)

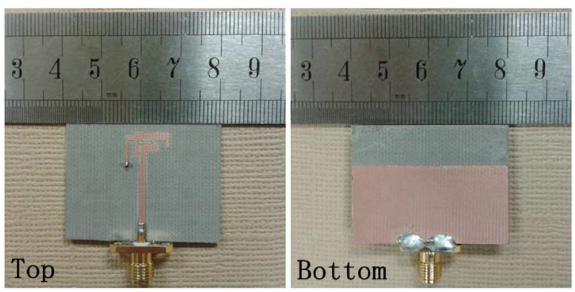

(c)

Fig. 1. (a) 3-D view of antenna. (b) Layout of radiator (A: feed point, G: via, prefixes W and L represent widths and lengths of elements). (c) prototyped antenna.

and is coupled-fed through the L-element. Since only one feed point is used for the two separate elements, the overall size is very compact. The antenna is designed and studied using the EM simulation tool CST. For verification, the antenna is fabricated and measured using the antenna measurement system, Satimo Starlab. The feeding cable used to connect the antenna to the measurement system affects the measurement results [20], resulting in some deviations from the simulation results. To study these effects, the feeding cable is also modeled and used in simulation. Then the simulation results agree very well with the measurement results. Moreover, the effects of housing and liquid crystal display (LCD) of wireless devices are also investigated in this paper.

II. Antenna Design

Fig. 1(a) shows the 3-D view of the proposed dual-band antenna which has a radiator with an area of 8×11.3 mm^2, a

TABLE I
Optimized Dimensions of Radiator (mm)

L1	3	*W1*	1.5	*L5*	1.55	*W5*	1
L2	3.25	*W2*	2	*L6*	9.15	*W6*	2
L3	4.5	*W3*	1	*L7*	2	*W7*	1
L4	6	*W4*	0.6	*g*	0.5		

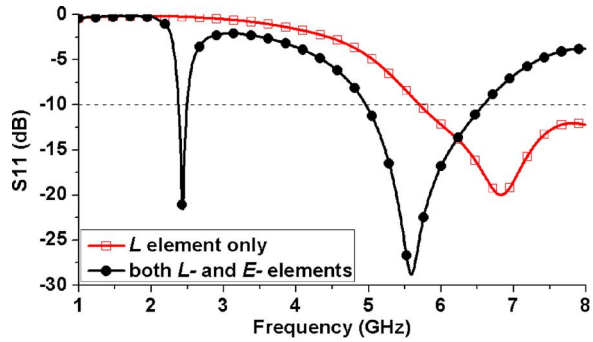

Fig. 2. Simulated S11 with only L-element and both L- and E-elements.

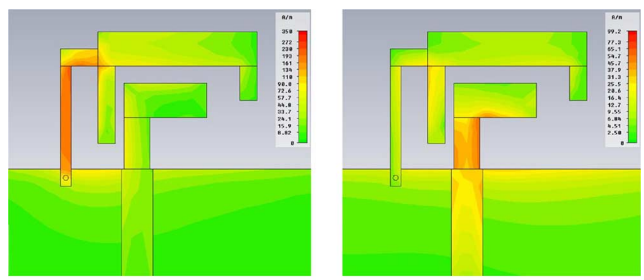

(a) (b)

Fig. 3. Simulated current distribution at (a) 2.44 GHz and (b) 5.5 GHz.

ground plane of 40×20 mm^2 and an overall dimensions of $40 \times 30 \times 0.8$ mm^3. The microstrip-feed line has a width of 1.8 mm to achieve a characteristic impedance of 50 Ω. (Note that the length of the feed line depends on the space available on the particular wireless device where the antenna is installed.) The geometry of the radiator is shown in Fig. 1(b) which consists of two radiating elements. These elements look like the letters E and L rotated by 90° and so are denoted here as an E- and L-elements, respectively. The prefixes W and L used to indicate the dimensions of Fig. 1(b) denote the widths and lengths, respectively, in different parts of the elements. The L-element is direct-fed by the feed line at "A" marked on Fig. 1(b). It generates a wide frequency band at 5.5 GHz for the higher WLAN bands at 5.2 and 5.8 GHz. The E-element, having a modified inverted-F structure, is coupled-fed from the L-element via the small gap g and is shorted to ground using a via with diameter of 0.3 mm marked as "G" on the shorting element of Fig. 1(b). It generates a band at around 2.44 GHz for the lower band of the WLAN system. Thus the antenna has dual-band operation to cover all the 2.4/5.2/5.8 GHz WLAN bands. Since only one feed point is required for the two separate elements which are closely packed together, the radiator size is very compact. The antenna is designed on a substrate with a relative permittivity of 3.5 and a loss tangent of 0.02, and optimized using computer

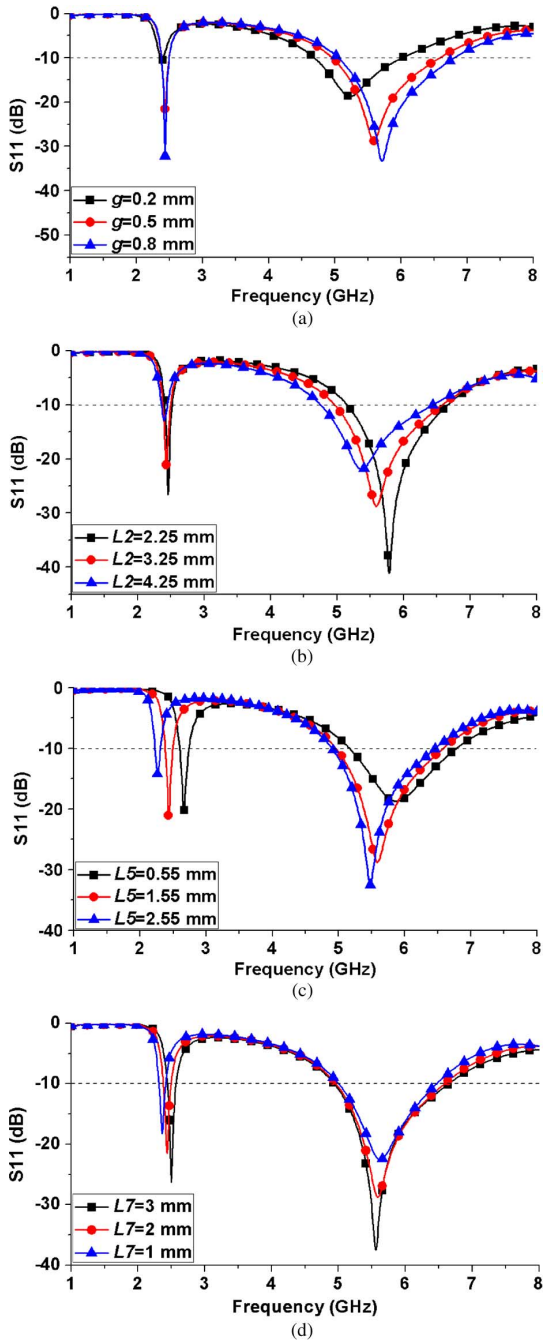

Fig. 4. Simulated S11 with different values of (a) g, (b) $L2$, (c) $L5$, and (d)$L7$.

simulation. The optimized dimensions are listed in Table I. The antenna is also fabricated as shown in Fig. 1(c) on a substrate with the same electrical parameters used in simulation.

III. Parameter Study

To study the resonant frequencies of the two radiating elements, the antenna with only the L-element present and with both elements present was studied using computer simulation. The results on the reflection coefficient S11 are shown in Fig. 2. It can be seen that, if only the L-element was present, the antenna resonated at a single frequency of about 7 GHz. When the E- element was added to the antenna, an additional mode was

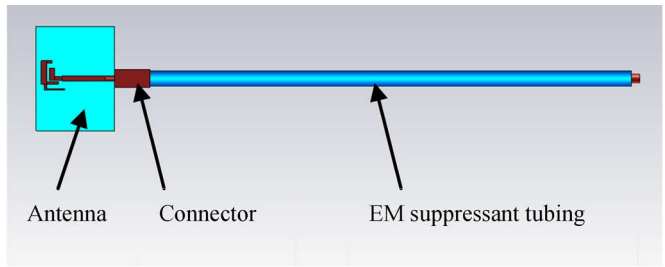

Fig. 5. Simulation model of antenna with EM suppressant tubing cable.

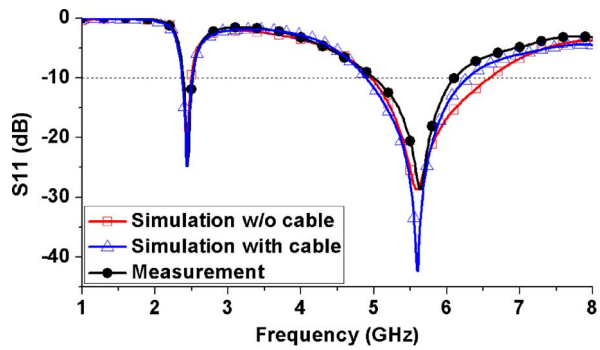

Fig. 6. Simulated and measured S11 of antenna.

generated at a lower frequency of 2.44 GHz and the resonance at 7 GHz was shifted down to around 5.5 GHz.

The operation of the antenna was further studied using current distributions at 2.44 and 5.5 GHz. At 2.44 GHz, the simulated result in Fig. 3(a) shows that the current was mainly on the E-element which contributed to resonance. While at 5.5 GHz, Fig. 3(b) shows that the current on the L-element was quite large, contributing to resonance.

Results of computer simulation showed that the antenna dimensions such as the coupling gap "g" between the two radiating elements, the $L2$ in the L-element and the $L5$ and $L7$ in the E-element were all quite sensitive to the resonant frequencies, so a parametric study was carried out on these dimensions using computer simulation. The S11 with $g = 0.2$, 0.5 and 0.8 mm is shown in Fig. 4(a). As the value of "g" increased, i.e. decreasing the coupling between the two radiating elements, both the lower and higher bands moved up, with the higher band moving more significantly. With "g" increased from 0.2 mm to 0.5 and 0.8 mm, the lower band moved from 2.39 GHz to 2.44 and 2.445 GHz, respectively, while the higher band moved significantly more from 5.23 GHz to 5.5 and 5.7 GHz. More importantly, matching for both lower and higher bands improved as g was increased from 0.2 to 0.8 mm. Thus g could be used to produce good matching for the two frequency bands.

The simulated S11 of the antenna with different values of $L2$ are shown in Fig. 4(b). Note that $L2 = 3.25$ mm is the optimized value listed in Table I for our design. Fig. 4(b) shows that $L2$ had strong effects on the frequency of the higher band, but very little effects on the lower band. With $L2 = 2.25$, 3.25, and 4.25 mm, the resonant frequencies for the higher band were 5.78, 5.5, and 5.37 GHz, respectively, but the lower band at 2.44 GHz was not affected much (simply because the L-element was responsible for resonance at around 5.5 GHz). These

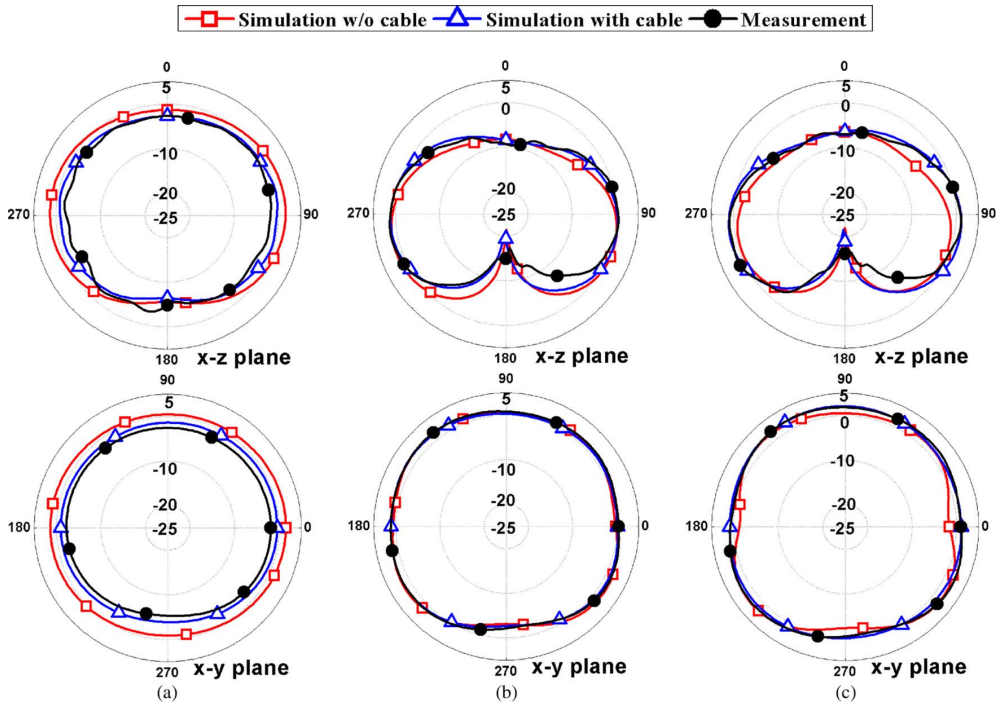

Fig. 7. Simulated and measured radiation patterns in $x-z$ and $x-y$ planes at (a) 2.44, (b) 5.2, and (c) 5.8 GHz.

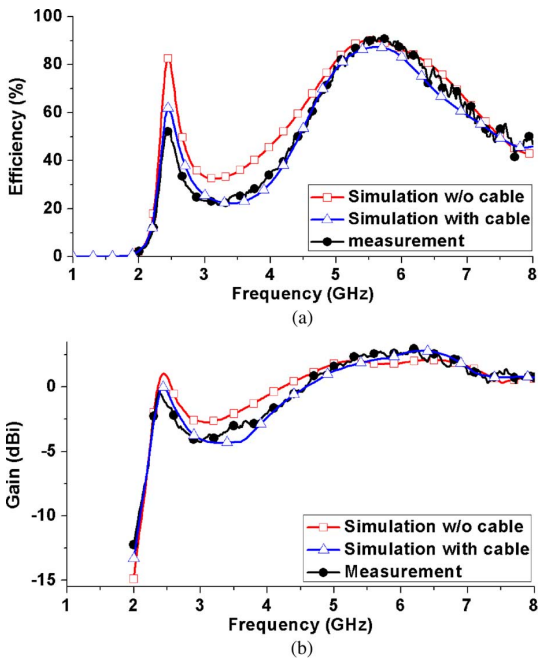

Fig. 8. Simulated and measured (a) efficiencies and (b) peak gains of antenna.

TABLE II
SIMULATED AND MEASURED EFFICIENCIES AND PEAK GAINS

Frequency (GHz)	Efficiency (%)		
	Sim. w/o cable	Sim. with cable	Meas.
2.44	83	62	52
5.2	87	84	85
5.8	89	87	89
	Gain (dBi)		
2.44	1	0	-0.9
5.2	1.98	1.6	1.95
5.8	1.8	2.2	2.32

results indicated that $L2$ could be used to independently tune the resonant frequency for the higher band.

The results of parametric study on $L5$ and $L7$ of the E-element are shown in Fig. 4(c) and (d). Fig. 4(c) shows that $L5$ had quite strong effects on the resonant frequencies for both the lower and higher bands. With $L5$ increased from 0.55 mm to 1.55 and 2.55 mm, the lower band moved from 2.67 GHz to 2.44 and 2.26 GHz, and the higher band moved from 5.86 GHz to 5.5 and 5.45 GHz, respectively. However, $L5$ did not affect much the bandwidth of the higher band, which was about 1.6 GHz (for S11 < -10 dB). Fig. 4(d) shows that $L7$ had some effects only on the lower band. With $L7 = 1$, 2, and 3 mm, the center frequencies for the lower band were 2.5, 2.44, and 2.36 GHz, respectively. For higher band, the resonant frequency and bandwidth remained about the same. These results indicated that $L5$ and $L7$ could be used to coarsely and finely, respectively, tune the resonant frequency of the lower band, without affecting much the higher band.

Based on these results obtained, the design methodology for the proposed dual-band antenna can be described as follows.

Step 1) For the L-element, set $L1 + L2 = \lambda_g/4$, with λ_g the guide wavelength at the high resonant frequency, and the ratio of $L1 : L2$ similar to the current design.

Step 2) For the E-element, set $L4 + L5 + L6 + L7 = \lambda_g/4$, where λ_g is the guide wavelength at the low resonant frequency, with the ratios of $L4 : L5 : L6 : L7$ similar to the current design.

Step 3) Set $gap = 0.5$ mm and other dimensions using Table I.

Step 4) The settings in *steps 1*, *2* and *3* will not produce exactly the high and low resonant frequencies, so

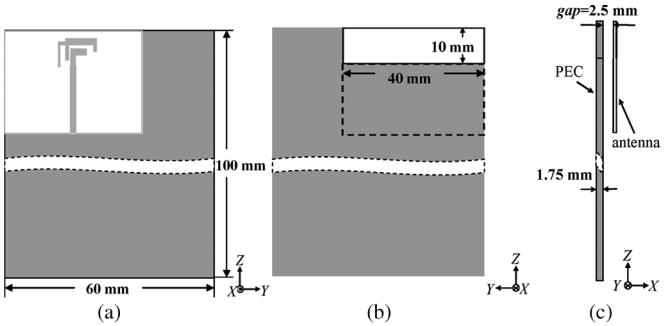

Fig. 9. Antenna with LCD model. (a) Front view. (b) Back view. (c) Side view.

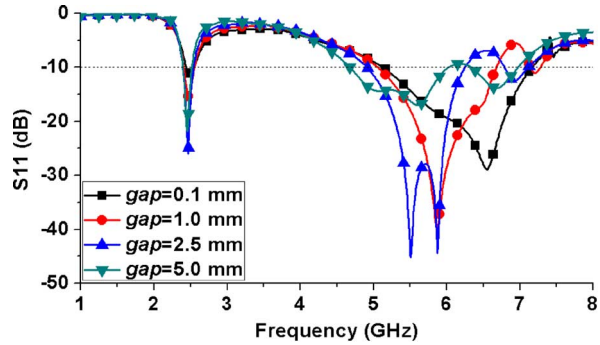

Fig. 10. Simulated S11 with different value of "gap".

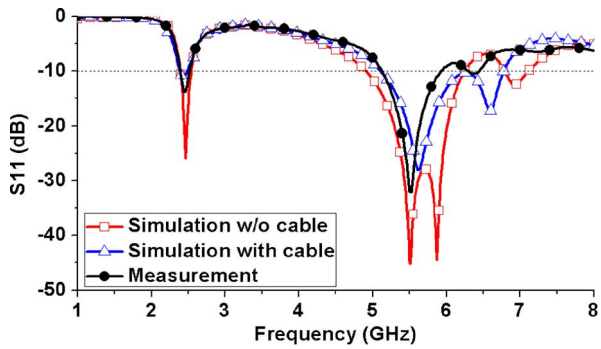

Fig. 11. Simulated and measured S11 with $gap = 2.5$ mm.

use $L7$ and $L2$ to fine tune the low and high bands, respectively.

Step 5) Optimize the matching using gap and the ratio $L5 : L6$ (yet keeping $L5 + L6$ unchanged).

IV. Simulation and Measurement Results

The S11 and radiation pattern of the antenna shown in Fig. 1(c) have been measured using the antenna measurement system, Satimo Starlab. When an antenna is placed in the Starlab for measurement, a coaxial feeding cable is always needed to connect the antenna to the system. In measuring small monopoles, at low frequencies where the electrical size of the antenna ground plane becomes relatively small compared to the wavelength, currents will flow back from the antenna to the feeding cable, giving rise to "secondary radiation" [20] and causing inaccuracy in radiated patterns measurement. This also alter the current distribution on the antenna and hence the S11. To reduce the effects on the measured radiation pattern, the feeding cable in the Starlab system is covered with EM suppressant tubing to absorb the currents flowing back to the cable and radiation from the cable. However, this method reduces the measured gain and efficiency of the antenna [21].

To study the cable effects on the measurement results, the antenna together with the feeding cable as shown in Fig. 5 was modeled in CST [21]. The cable had a length of 186.5 mm and was covered with EM suppressant tubing having thickness of 1.25 mm, relative permittivity of 5, relative permeability of 5, loss tangent of 0.004 and magnetic loss tangent of 0.3. A metallic block with a size of $6.5 \times 6.5 \times 13.5$ mm_3 was used to model the SMA connector. (Simulation showed that a cable length of longer than 400 mm would produce the similar results, so a length of 186.5 mm was used to reduce simulation time).

The simulated and measured S11 are show in Fig. 6. It can be seen that, at 5.5 GHz, the simulation result without using the cable model had a wider bandwidth than that of the measurement result. With the use of the feeding cable, the simulation results and measurement results had a much better agreement. The measured bandwidths $(\mathrm{S11} < 10\ \mathrm{dB})$ for the lower band was from 2.39 to 2.51 GHz and for the higher band was from 5 to 6.1 GHz, with both bands satisfying the requirements of the WLAN standards.

The simulated radiation patterns of the antenna with and without using the cable at 2.44, 5.2, and 5.8 GHz in the x–z and x–y planes are shown in Fig. 7. For comparison, the corresponding measured radiation patterns are also shown in the same figures. Fig. 7(a) shows that, at the lower frequency of 2.44 GHz, the simulation results without using the cable in general had the largest gains, for the reasons described previously. With the use of the measuring cable, the simulation results and measurement results had better agreements. Moreover, the antenna had omnidirectional radiation patterns in both the x–z and x–y planes, which were similar to those of invert-F-like antenna. At the higher frequencies of 5.2 and 5.8 GHz, Fig. 7(b) and (c) show that both the simulation results with and without using the cable agreed well with the measurement results. This was because at higher frequencies, the cable effects were less significant due to the increased electrical size of the antenna ground plane. The antenna had omnidirectional radiation patterns in the x–y plane and a dip at the z-direction in the x–z plane, which was similar to those of inverted-L-like antenna.

The simulated and measured efficiencies and peak gains of the antenna are shown in Fig. 8, with the numerical results at 2.44, 5.2, and 5.8 GHz listed in Table II. When the feeding cable was used in simulation, the simulated and measured results agreed very well. Here the small discrepancies were mainly due to 1) the parameters used to model the EM suppressant tubing were not exact or constant across the frequency band, and 2) the dimensions of the SMA connector and the cable length were not exact. Fig. 8(a) shows that the simulated efficiencies without using the feeding cable were always highest and the discrepancies between the simulated and measured results were larger at lower frequencies, for the reasons of cable effects described previously. Fig. 8(b) and Table II show that the measured peak gain was smaller than the simulated gain without using the cable model at 2.44 and 5.2 GHz, but larger at 5.8 GHz.

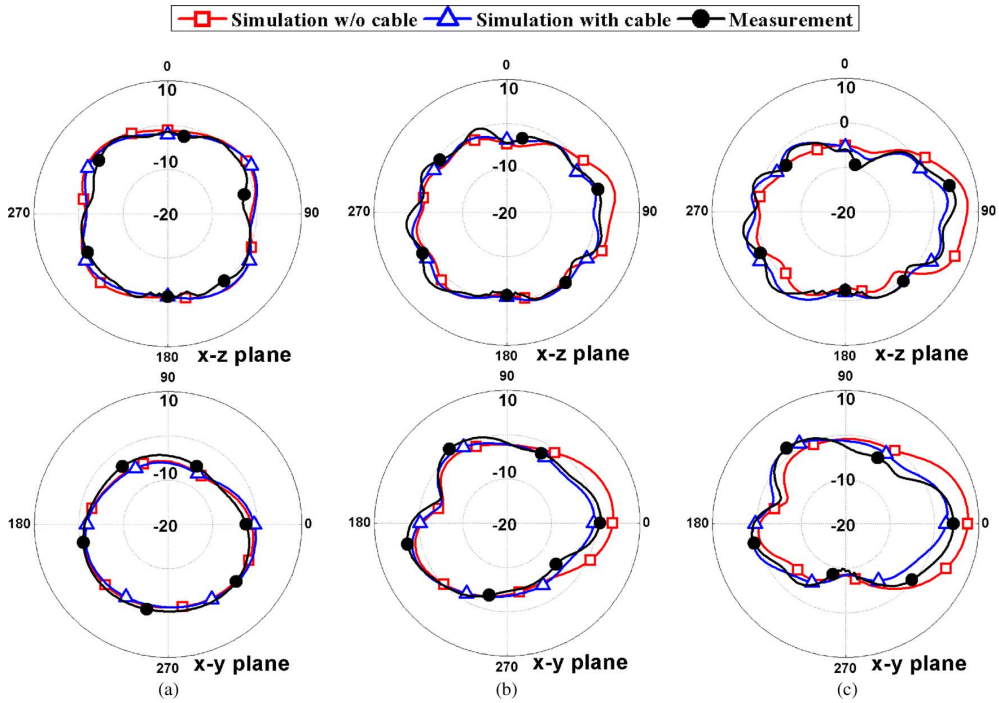

Fig. 12. Simulated and measured radiation patterns using LCD in x–z and x–y planes at (a) 2.44, (b) 5.2, and (c) 5.8 GHz.

Simulation on the 3-D radiation patterns was carried out to study the reason for this. Results showed that at 5.8 GHz, the cable effects changed the direction of the main lobe on the radiation pattern and made it more directional with a higher gain. This effect could not be seen in Fig. 7(c) because the main lobe was not in the x–z or x–y planes. Due to the page limit, the 3-D patterns are not shown here.

V. Effect of Nearby Conductor and Device Housing

Although the antenna has been designed using simulation and measurement, when the antenna is installed in a wireless device, the performance will be affected by the nearby conductors and the housing. Nowadays, wireless devices such as smart phones often have a large liquid-crystal display (LCD) mounted on a metal plate. Under the LCD, it is a PCB with electronics components mounted on it. The phone antenna is often installed on the metal plate and covered by housing. For installing a planar monopole antenna, a small area of the metal plate is normally removed, as shown in Fig. 9, to avoid interference with the antenna. To study such condition for the proposed antenna, a perfect electric conductor (PEC) with size of $100 \times 60 \times 1.75$ mm^3 as shown in Fig. 9 was used to model the LCD in CST. There was a gap between the antenna and the LCD. (In practice, the antenna ground plane could be connected directly to the LCD without have this gap, but then our antenna needed to be redesigned because of the larger ground. For convenience, we used the same antenna for studies.) Simulation and measurement were used to study the effects of the LCD on the S11, radiation pattern, gain and efficiency.

With $gap = 0.1$, 1, 2.5, and 5 mm between the LCD and the antenna, the simulated S11 is shown in Fig. 10. It can be seen that, with all the tested values for gap, the antenna could cover the WLAN bands. However, due to the physical size of the SMA connector attached to the antenna, the smallest gap size which could be used for measurement was $gap = 2.5$ mm.

With $gap = 2.5$ mm, the simulated and measured S11 are shown in Fig. 11. To evaluate the cable effects on the S11, the simulated S11 using the cable model is also shown in the same figure. It can be seen that the simulated S11 using the cable model had a better agreement with the measured S11. The measured bandwidth for the lower band remained about the same from 2.39 to 2.5 GHz. For the higher band, the measured bandwidth was from 5 to 6.06 GHz, slightly narrower than that (in Fig. 6) without having the LCD. An additional resonance at around 6.5 GHz was generated by the LCD.

Using the LCD model, the simulated and measured radiation patterns at 2.44 GHz are shown in Fig. 12(a). The antenna still had quite omnidirectional radiation patterns in the x–z and x–y planes. Without using the cable model and at 5.2 and 5.8 GHz, Fig. 12(b) and (c) show the antenna has slightly directional radiation patterns at the x-direction. However, with the cable model, the radiation patterns at these two frequencies in Fig. 12(b) and (c) were less directional in both the x–z and x–y planes. The simulation results using the cable model were slightly closer to the measured results.

With $gap = 2.5$, Fig. 13 shows the simulated and measured efficiencies and peak gains. The simulated results with using the cable model agreed very well with the measured results. At the frequencies of 2.44, 5.2, and 5.8 GHz, the measured efficiencies were 66.8%, 83.6%, and 85%, respectively, with the corresponding measured gains of 1.66, 4.75, and 5.1 dBi.

The effects of having housing on the antenna were also studied using the simulation model shown in Fig. 14. The housing had a thickness of 1 mm and was made of Acrylonitrile Butadiene Styrene with a relative permittivity of 2.3. Since the antenna was only affected by the material surrounding it, to

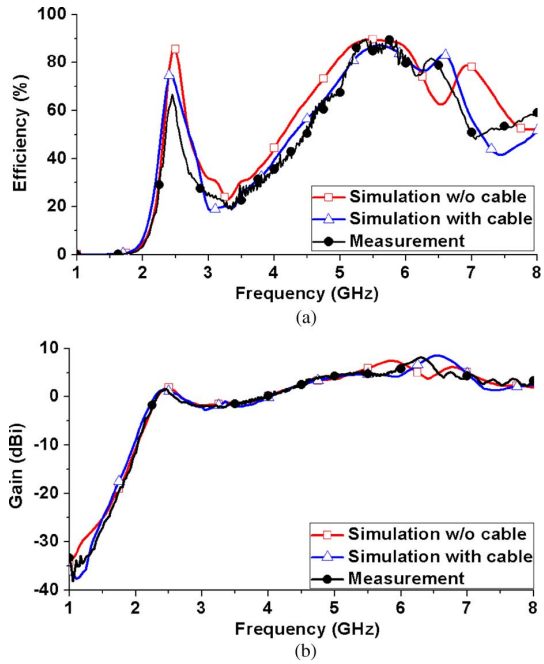

Fig. 13. Simulated and measured (a) efficiencies and (b) peak gains of antenna with $gap = 2.5$ mm.

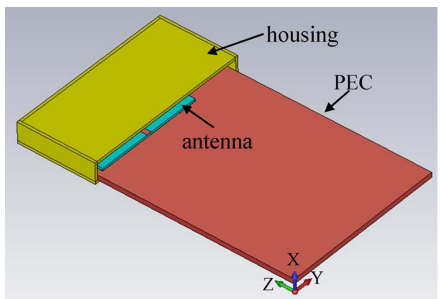

Fig. 14. Simulation model for antenna on LCD and surrounded by housing.

reduce the simulation time, the housing in the model of Fig. 14 covered only the antenna.

The simulated S11 with the LCD and housing models is shown in Fig. 15. For comparison, the simulated S11 without having the LCD or housing is also shown in the same figure. Both frequency bands were slightly shifted to lower frequencies. This was because the housing material with a higher dielectric constant decreased the wavelength and so decreased the frequencies. The bandwidth for the higher band was from 4.75 to 6 GHz, which was still large enough to cover the two higher bands for the WLAN system. However, the bandwidth for the lower band was from 2.3 to 2.43 GHz, which could not cover the lower band of the WLAN system. Since Fig. 4(d) showed that the lower band could be independently tuned using $L7$, the antenna was redesigned and optimized with using the LCD and housing. With an optimum value of $L7 = 0.8$ mm, the simulated S11 is shown in Fig. 15. It can be seen that the lower band was shifted slightly higher, with a bandwidth from 2.37 to 2.51 GHz, large enough for the lower band of the

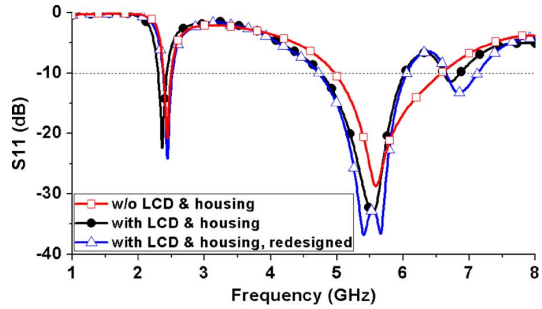

Fig. 15. Simulated S11 with LCD and housing model.

WLAN system. In doing this, there was not much change in the higher band.

VI. Conclusions

A dual-band monopole antenna with a very compact area of only 8×11.3 mm^2 for 2.4/5.2/5.8-GHz WLAN applications has been designed and studied using computer simulation and measurement. The antenna radiator consists of an L-shaped and E-shaped elements having resonances at about 2.44 and 5.5 GHz, respectively. The two frequency bands can be tuned independently. The S11, radiation pattern, gain and efficiency all have been studied.

The feeding cable used in the measurement equipment has been modeled using computer simulation. The simulation results using the feeding cable agree very well with the measurement results.

The antenna has also been studied using the simulation models for the LCD and housing. Results have shown that the antenna is a very promising candidate for practical WLAN applications.

References

[1] T. N. Chang and J. J. Jiang, "Meandered T-shaped monopole antenna," *IEEE Trans. Antennas Propag.*, vol. 57, no. 12, pp. 3976–3978, Dec. 2009.

[2] Q. X. Chu and L. H. Ye, "Design of compact dual-wideband antenna with assembled monopoles," *IEEE Trans. Antennas Propag.*, vol. 58, no. 12, pp. 4063–4066, Dec. 2010.

[3] S. H. Yeh and K. L. Wong, "Dual-band F-shaped monopole antenna for 2.4/5.2 GHz WLAN application," in *IEEE Antenna Propag. Soc. Int. Symp. Dig.*, 2002, vol. 4, pp. 72–75.

[4] Y. F. Lin, H. D. Chen, and H. M. Chen, "A dual-band printed L-shaped monopole for WLAN applications," *Microw. Opt Technol. Lett.*, vol. 37, pp. 214–216, 2003.

[5] T. H. Kim and D. C. Park, "CPW-fed compact monopole antenna for dual-band WLAN applications," *Electron. Lett.*, vol. 41, pp. 291–293, 2005.

[6] W. C. Liu, "Wideband dual-frequency double inverted-L CPW-fed monopole antenna for WLAN application," *IEE Proc. Microw., Antennas Propag.*, vol. 152, pp. 505–510, 2005.

[7] B. S. Yildirim, "Low-profile and planar antenna suitable for WLAN/Bluetooth and UWB applications," *IEEE Antenna Wireless Propag. Lett.*, vol. 5, pp. 438–441, 2006.

[8] C. M. Wu, C. N. Chiu, and C. K. Hsu, "A new non-uniform meandered and fork-type grounded antenna for triple-band WLAN applications," *IEEE Antenna Wireless Propag. Lett.*, vol. 5, pp. 346–348, 2006.

[9] R. D'Souza and R. K. Gupta, "Printed dual band WLAN antenna," in *Proc. IEEE Int. Conf. Electron. Inf. Technol.*, 2006, pp. 539–543.

[10] S. C. Basaran and Y. E. Erdemli, "A dual-band split-ring monopole antenna for WLAN applications," *Microw. Opt Technol. Lett.*, vol. 51, no. 11, pp. 2685–2688, 2009.
[11] S. W. Su, "High-gain dual-loop antennas for MIMO access points in the 2.4/5.2/5.8 GHz bands," *IEEE Trans. Antennas Propag.*, vol. 58, no. 7, pp. 2412–2419, Jul. 2010.
[12] Y. C. Lee and J. S. Sun, "Compact printed slot antennas for wireless dual- and multi-band operations," *Progress Electromagn. Res.*, vol. 88, pp. 289–305, 2008.
[13] D. Lin, Y. L. Zhen, Y. J. Xie, L. N. Gao, and J. Fan, "A compact mircostrip slot triple-band antenna for WLAN/WiMAX applications," *IEEE Antennas Wireless Propag. Lett.*, vol. 9, pp. 1178–1181, 2010.
[14] M. Z. Azad and M. Ali, "A miniature implanted inverted-F antenna for GPS application," *IEEE Trans. Antennas Propag.*, vol. 57, no. 6, pp. 1854–1858, Jun. 2009.
[15] M. Gallo, O. Losito, V. Dimiccoli, D. Barletta, and M. Bozzetti, "Design of an inverted F antenna by using a transmission line model," in *Proc. 5th Eur. Conf. Antennas Propag.*, 2011, pp. 635–638.
[16] D. X. Liu and B. Gaucher, "The inverted-F antenna height effects on bandwidth," *Proc. IEEE Antennas Propag. Soc. Int. Symp.*, vol. 2A, pp. 367–370, 2005.
[17] T. H. Jiang, D. L. Su, K. J. Ding, G. Y. Wang, and Y. Zhou, "Design of the low-profile inverted-F antenna with multiparasitic elements," in *Proc. 7th Int. Symp. Antennas, Propag. EM Theory*, 2006, pp. 1–4.
[18] A. R. Razali and M. E. Bialkowski, "Coplanar inverted-F antenna with open-end ground slots for multiband operation," *IEEE Antenna Wireless Propag. Lett.*, vol. 8, pp. 1029–1032, 2009.
[19] H. Y. Wang and M. Zheng, "An internal triple-band WLAN antenna," *IEEE Antennas Wireless Propag. Lett.*, vol. 10, pp. 569–572, 2011.
[20] C. Icheln, "Methods for Measuring RF Radiation Properties of Small Antennas," Ph.D. dissertation, Dept. Elect. Commun. Eng., Helsinki Univ. Technol., Espoo, Finland, Nov. 2001.
[21] L. Liu, Y. F. Weng, S. W. Cheung, T. I. Yuk, and L. J. Foged, "Modeling of cable for measurements of small monopole antennas," presented at the Loughborough Antennas Propag. Conf. (LAPC 2011), Loughborough, U.K., Nov. 14–15, 2011.

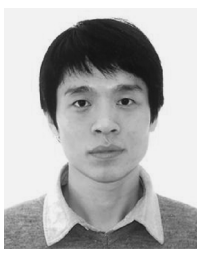

Xiao Lei Sun received the B.S.E.E. degree from the Huazhong University of Science and Technology, Wuhan, China, in 2005, and the M.S. degree in microelectronics and solid-state electronics from the Institute of Microelectronics, Chinese Academy of Sciences, Beijing, China, in 2008. He is currently working toward the Ph.D. degree at the department of electrical and electronic engineering, The University of Hong Kong, Hong Kong, China.

His research interests include high power amplifier linearization, RF and microwave circuits, multiband antennas, and frequency tunable antennas.

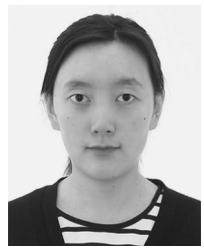

Li Liu received the B.Sc. degree from the University of Electronic Science and Technology of China, Chengdu, China, in 2008. She is currently working toward the Ph.D. degree at the University of Hong Kong, Hong Kong, China.

Her research interests include RF and microwave circuits, UWB antennas and multiband antennas.

S. W. Cheung (SM'98) received the B.Sc. degree (first class honors) in electrical and electronic engineering from Middlesex University, London, U.K., in 1982, and the Ph.D. degree from Loughborough University of Technology, Loughborough, U.K., in 1986.

From 1982 to 1986, he was a Research Assistant in the Department of Electronic and Electrical Engineering, Loughborough University of Technology, where he collaborated with Rutherford Appleton Laboratory and many U.K. universities to work a project for new generations of satellite systems. From 1986 and 1988, he was a postdoctorate Research Assistant with the Communications Research Group of King's College, London University, working on research for future generations of satellite systems. In 1988, he joined the Radio and Satellite Communications Division in British Telecom Research Laboratories (now British Telecom Laboratories), as an Assistant Executive Engineer. He is an Associate Professor at the University of Hong Kong and in charge of the Microwave, RF Frequency, and Telecom Laboratories. He has published over 150 technical papers in international journals and conferences in these areas. His current research interests include antenna designs, 2-, 3-, and 4G mobile communications systems, MIMO systems and satellite communications systems, predistortion of high power amplifiers and e-learning.

Dr. Cheung has served the IEEE in Hong Kong for the past 20 years. In 2009 and 2010, he was the Chairman of the IEEE Hong Kong Joint Chapter on Circuits and Systems and Communications. Since 2011, he has been the Treasurer of the IEEE Hong Kong Section and help organizing different international conferences. He also has served as Reviewer for different international journals and conferences in the areas of antennas and propagation and mobile communications.

T. I. Yuk received the B.S. degree from Iowa State University, Ames, IA, in 1978, and the M.S. and Ph.D. degrees from Arizona State University, Tuscan, in 1980 and 1986 respectively.

Since 1986, he has been teaching at the University of Hong Kong, Hong Kong , China. His current research interests include wireless communications and antenna designs.